Guiding of Charged Particle Beams in Curved Plasma-Discharge Capillaries

R. Pompili,[1,*] M. P. Anania,[1] A. Biagioni,[1] M. Carillo,[2] E. Chiadroni,[2] A. Cianchi,[3,4,5] G. Costa,[1] A. Curcio,[1] L. Crincoli,[1] A. Del Dotto,[1] M. Del Giorno,[1] F. Demurtas,[3] A. Frazzitta,[2,6] M. Galletti,[3,4,5] A. Giribono,[1] V. Lollo,[1] M. Opromolla,[1] G. Parise,[3] D. Pellegrini,[1] G. Di Pirro,[1] S. Romeo,[1] A. R. Rossi,[6] G. J. Silvi,[2] L. Verra,[1] F. Villa,[1] A. Zigler,[7] and M. Ferrario[1]

[1]*Laboratori Nazionali di Frascati, Via Enrico Fermi 54, 00044 Frascati, Italy*
[2]*University of Rome Sapienza, Piazzale Aldo Moro 5, 00185 Rome, Italy*
[3]*University of Rome Tor Vergata, Via della Ricerca Scientifica 1, 00133 Rome, Italy*
[4]*INFN Tor Vergata, Via della Ricerca Scientifica 1, 00133 Rome, Italy*
[5]*NAST Center, Via della Ricerca Scientifica 1, 00133 Rome, Italy*
[6]*INFN Milano, via Celoria 16, 20133 Milan, Italy*
[7]*Racah Institute of Physics, Hebrew University, 91904 Jerusalem, Israel*

(Received 18 December 2023; accepted 1 May 2024; published 22 May 2024)

We present a new approach that demonstrates the deflection and guiding of relativistic electron beams over curved paths by means of the magnetic field generated in a plasma-discharge capillary. We experimentally prove that the guiding is much less affected by the beam chromatic dispersion with respect to a conventional bending magnet and, with the support of numerical simulations, we show that it can even be made dispersionless by employing larger discharge currents. This proof-of-principle experiment extends the use of plasma-based devices, that revolutionized the field of particle accelerators enabling the generation of GeV beams in few centimeters. Compared to state-of-the-art technology based on conventional bending magnets and quadrupole lenses, these results provide a compact and affordable solution for the development of next-generation tabletop facilities.

DOI: 10.1103/PhysRevLett.132.215001

Particle accelerators represented a key engine for a wide range of discoveries and, since their introduction, started a new era for a breakthrough perspective of the microscopic world at the subatomic level [1] and subfemtosecond timescale [2]. Considering the increasing demands in terms of beam energy, compactness, and low-cost operation, new accelerators based on plasma became very attractive [3], with many pioneering experiments that generated GeV beams in few centimeters [4–9]. Moreover the impressive advances on the beam quality [10–12] made plasma technology very competitive even for user-oriented applications [13–16]. However, while tremendous progress was achieved by reducing the accelerator size, particle beams are still handled and transported with conventional bending and quadrupole magnets [17]. The state of the art is represented by devices relying on permanent magnets [18,19] and superconductors operating at cryogenic temperatures [20,21]. The latter technology is used, for instance, at the Large Hadron Collider (LHC) [22] but requires complex and expensive cryogenic systems. Looking toward the development of futuristic ultracompact machines, a breakthrough concept must be therefore envisioned.

Here, we report about a proof-of-principle experiment where we employed a curved plasma-discharge device to bend and guide a relativistic electron beam [23]. Such a device, hereinafter called active-bending plasma (ABP) and shown in Fig. 1(a), consists of a capillary tube filled up with nitrogen gas with length $L_c = 10$ cm and bending radius $R_{\mathrm{bend}} \approx 1.6$ m. The deflection is obtained by applying a high-voltage discharge current to the two electrodes connected at its ends. The discharge generates the plasma and,

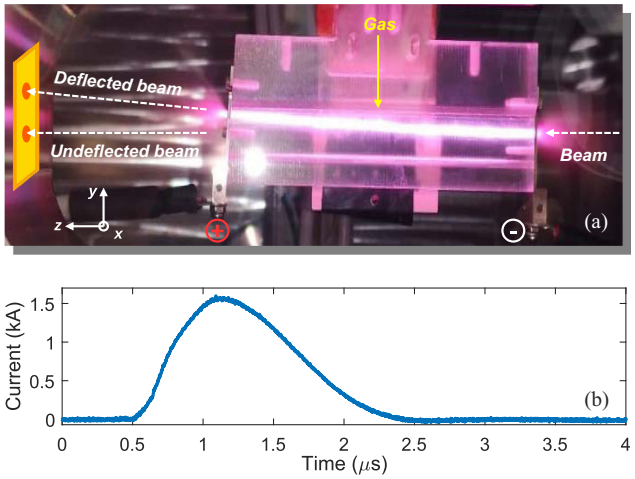

FIG. 1. (a) Experimental setup. The high-voltage discharge current is applied to the two electrodes of the curved capillary to produce the plasma. The beam is measured on a scintillating screen located 10 cm downstream of it. The orientation of the x-y-z axes is also indicated. (b) Discharge current waveform acquired with a digital scope.

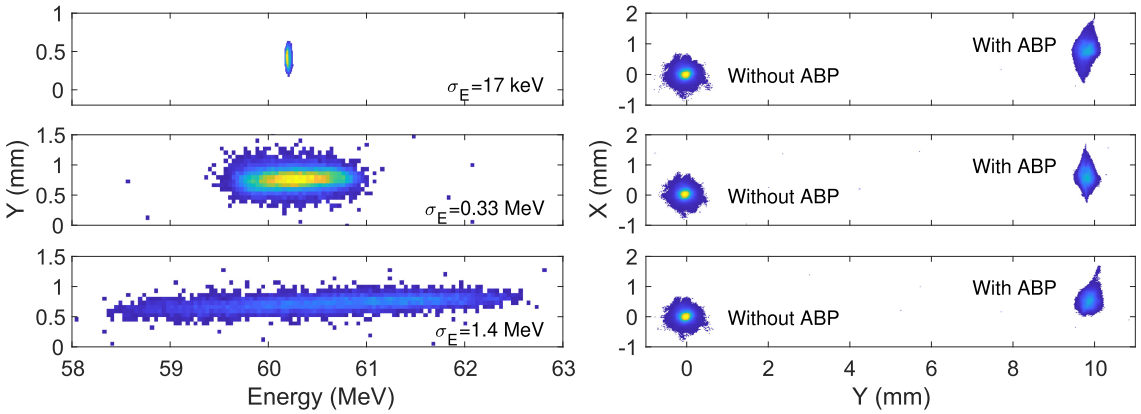

FIG. 2. Proofs of beam deflection. Left column: energy spectra of the beam obtained for three different working points of the linac. The corresponding energy spreads σ_E are indicated in each plot. Right column: deflected and undeflected transverse spot sizes downstream of the ABP. Each plot is obtained by overlapping a single shot of the undeflected beam (capillary out of the beam path) with a single shot of the deflected one (capillary inserted and discharge current set to $I_D \approx 1.57$ kA). The energy spread is the same as in the corresponding spectrum on the left.

in turn, the poloidal magnetic field [24] that simultaneously focuses and guide the beam over the curved path providing an overall 4° deflection on the vertical plane. We experimentally show that, with respect to a conventional bending magnet (CBM), the guiding is less affected by the beam chromatic dispersion and, according to numerical simulations, can even be made *dispersionless* by tuning the discharge current.

The experiment is carried out at the SPARC_LAB facility [25] by using a 50 pC electron beam with $E = 60.2 \pm 0.1$ MeV energy, $\sigma_t = 0.9 \pm 0.1$ ps duration, and $\epsilon_r = 0.6 \pm 0.1$ μm normalized emittance. The transverse spot size at the capillary entrance is $\sigma_r = 130 \pm 10$ μm (rms) and its time of arrival jitter is ≈50 fs [26]. The diagnostics station consists of a cerium-doped gadolinium aluminum gallium garnet scintillating screen located 10 cm downstream of the capillary. The light emitted by the screen is collected into a CCD camera with 20.2 μm pixel resolution. The ABP is 3D-printed using a photopolymeric material and has a 2 mm hole diameter and $L_c = 10$ cm length with its input and exit apertures, which are displaced by 3 mm on the vertical plane where the bending is performed. The capillary is installed in a vacuum chamber directly connected with a windowless, three-stage differential pumping system that ensures 10^{-8} mbar pressure in the rf linac while flowing the gas. This solution allows one to transport the beam without encountering any window, thus not degrading its emittance by multiple scattering. A high-speed solenoid valve is used to fill the capillary with nitrogen gas through one inlet located at $L_c/2$. The discharge current, whose waveform is shown in Fig. 1(b), is provided by a 20 kV generator that provides pulses with peak current $I_D \approx 1.57$ kA and ≈1 μs duration (FWHM). The discharge timing jitter is about 1 ns [27,28]. The average plasma density along the ABP, measured with Stark-broadening diagnostics [29], is $n_p \approx 2.5 \times 10^{17}$ cm^{-3}.

The ABP guiding is demonstrated by testing its operation with three different beam configurations. We tuned the rf linac to produce a low ($\sigma_E = 17 \pm 1$ keV), medium ($\sigma_E = 0.33 \pm 0.01$ MeV), and large ($\sigma_E = 1.4 \pm 0.2$ MeV) energy spread while keeping fixed the average beam energy. Figure 2 (left column) shows the energy spectra of such beams measured with a magnetic spectrometer and the resulting beam spot sizes (right column) obtained on the scintillating screen downstream of the ABP. The deflection is achieved by applying a discharge current $I_D \approx 1.57$ kA. To compare the undeflected and the deflected beam we overlapped two single-shot images obtained without the ABP (capillary removed from the beam path) and with the ABP (capillary centered on the beam path with the discharge turned on). The plots show that the beam is guided along the curved path and, after traveling on the following drift, reaches the screen with an overall displacement $\Delta Y = 9.9 \pm 0.1$ mm.

We performed a parametric scan to characterize the ABP deflection for all the three beam configurations by varying the applied discharge current. Figure 3 shows the resulting spot sizes measured on the screen for several discharge currents in the range $I_D \approx 1.29 \div 1.57$ kA, with each point obtained as the average of 100 consecutive single-shot images. The last plot also reports the percentage of transmitted charge obtained as the ratio between the CCD counts with the ABP turned on and the counts when the capillary is removed from the beam path. The plot shows that, as expected, the beam guiding efficiency is enhanced at large discharge currents, with the output charge that reaches up to ≈100%. On the contrary, when the discharge is turned off, no charge is transmitted since the input and output apertures are not aligned and the beam is damped in the capillary walls. An interesting feature is that the deflected spot sizes show a negligible dependency on the beam energy spread, especially when the discharge current is

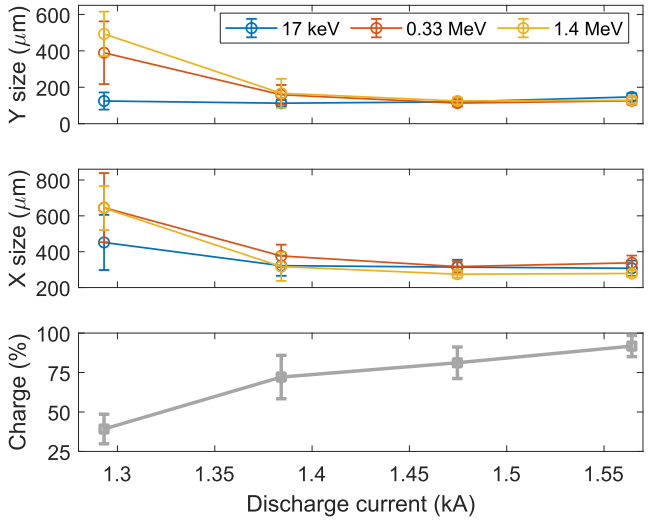

FIG. 3. Transverse spot sizes of the deflected beam. The first two plots show the X/Y spot sizes for several discharge currents respectively. Each point is obtained by averaging 100 consecutive single shots, with the error bar computed as their standard deviation. The third plot reports the average percentage of transmitted beam charge downstream of the capillary with respect to the undeflected one, retrieved by summing the counts of the acquired CCD images.

large enough. This indicates that the effects of the beam chromatic dispersion are reduced if compared with a conventional bending magnet. At this regard, we provide in the following a theoretical study by means of numerical simulations to describe the beam dynamics in the ABP and, for the sake of completeness, we compare it with an equivalent CBM having the same length and bending radius.

To understand the guiding mechanism of the ABP it is fundamental to know how its magnetic field acts on the beam. This is showed in Fig. 4(a), where we evaluate the ABP field assuming $I_D = 1.57$ kA. The field is computed with a one-dimensional analytical model that takes into account the radial plasma temperature profile to retrieve the current density $J_D(r)$ flowing in the capillary and, in turn, the induced magnetic field as $B_{\mathrm{ABP}} = \mu_0/r \cdot \int_0^r J_D(r')r'dr'$ [30,31]. The field is poloidal, increases with radius, and is focusing everywhere (the discharge current flows in the same direction of the beam) so that particles farther from the axis experience a stronger focusing effect. The beam dynamics is thus different from a CBM, whose field is unidirectional and constant with magnitude $B_{\mathrm{CBM}} = E[\mathrm{MeV}]/(c \cdot R_{\mathrm{bend}}) \times 10^6 \approx 0.13$ T. The trajectories followed by the beam particles are indeed different in the two cases, especially for the largest energy spread $\sigma_E = 1.4$ MeV configuration, where the effects of the chromatic dispersion on the bending plane become evident. This is showed in Fig. 4(b) where the evolution of 1000 particles is tracked including the drift section downstream of the bending device.

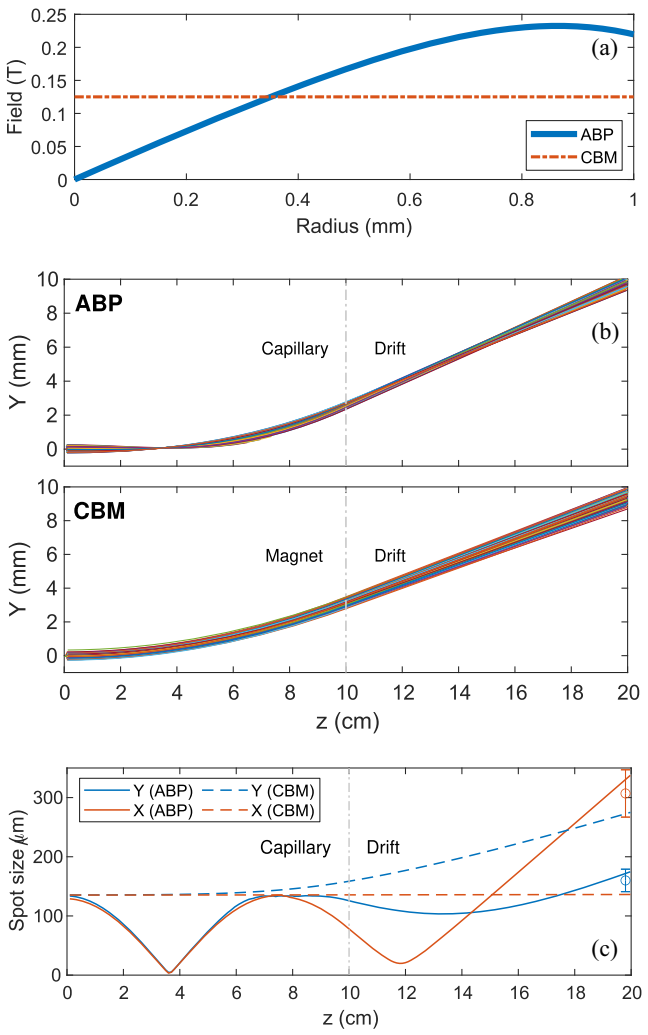

FIG. 4. Comparison between ABP and CBM. (a) Magnetic field computed as a function of the radial distance from capillary axis. (b) Particles trajectories along the ABP (top) and CBM (bottom) including the following drift up to the measurement screen for the beam with $\sigma_E = 1.4$ MeV energy spread. (c) Corresponding horizontal and vertical beam envelope evolution. The dot-dashed gray line shows the start of the drift space. The circle data points with error bars refer to the experimentally measured spot sizes with the ABP.

The corresponding beam envelopes are reported in Fig. 4(c). The beam initially focuses in the ABP, reaching a waist after ≈4 cm and then is guided up to the capillary exit. Particles with larger energies can travel more off-axis with respect to the lower energy ones but, since the focusing field increases with radius, they experience a stronger focusing force. As a result, the spread of the trajectories on the bending plane (due to chromatic dispersion) is reduced with respect to a CBM where particles with larger (smaller) energies are less (more) deflected by the constant field. In the latter case the increase of the spot size is therefore more pronounced. This is confirmed in Fig. 4(c) where the vertical spot size at the

ABP exit is ≈30% smaller than the one at the CBM exit and ≈65% including the drift section.

Considering the chromatic dispersion, it is interesting to compare again the ABP with the CBM. Mathematically the dispersion is represented by the R_{16} term of the linear transport matrix $\mathbf{R}$ [32] that links the beam particle position y_i with its momentum error $\delta E_i = (E_i - E)/E$. For a CBM with length $L_{\mathrm{CBM}} = L_c$ such a quantity is analytically given by $R_{16} = R_{\mathrm{bend}}(1 - \cos(L_{\mathrm{CBM}}/R_{\mathrm{bend}})) \approx 3.1$ mm. Figure 5(a) shows the resulting particle distribution in the case of ABP and CBM, respectively. A linear fit is computed on each distribution with its slope that corresponds to the R_{16} term. As expected the chromatic dispersion is smaller in the ABP and, as shown in Fig. 5(b), can even be tuned by varying the discharge current I_D. We considered discharge currents as large as 17 kA but in principle this value can be increased, e.g., up to $I_D \approx 60$ kA [33,34]. The plot indicates that the ABP dispersion can be largely adjusted to achieve both positive and negative values and, for specific discharge currents, it can be made zero. Such a feature is very attractive since it allows, with a single device, one to displace the dispersionless beam over an arbitrary path without requiring two bending magnets with dispersion-matching optics in between like quadrupoles and sextupoles [35].

Regarding the scalability of the ABP to larger beam energies, we considered the scenario envisioned by EuPRAXIA [36] that foresees the realization of a plasma-based accelerator facility providing electron beams with ≈1 GeV energy [37]. We demonstrate that the ABP operation can be extended to such beam parameters by adjusting the discharge current and capillary geometry. Figure 5(c) shows the guiding efficiency obtained for an ABP with the same capillary length L_c and bending radius R_{bend} used in the experiment. The plot shows the percentage of transported charge along the curved path as a function of the input discharge current. As previously discussed, the increase of I_D enhances the overall transport efficiency. However, the guiding can also be improved by narrowing the capillary hole diameter since it allows one to increase the corresponding current density J_D and, in turn, the peak magnetic field. In such a way the same efficiency can be obtained with a smaller I_D. It is worth noticing, however, that the operation at very large peak currents will require a proper cooling system to counteract the total energy that is deposited and, in turn, the rise of temperature in the capillary walls.

In conclusion, we presented a new concept based on a curved discharge capillary able to deflect and guide a relativistic electron beam. The results of such a proof-of-principle experiment demonstrate the effectiveness of its deflection on a 60 MeV electron beam. The measurements have been validated with a theoretical study showing that the guiding can be tuned by adjusting the discharge current. This allows one also to change the chromatic dispersion of the ABP that can be ideally made dispersionless, a unique feature not available in conventional bending magnets employed so far. The adjustment of the discharge current and/or capillary geometry allows one also to extend the ABP operation to larger beam energies, allowing its implementation for a wide range of applications. If compared to state-of-the-art bending magnets technology, its practical implementation would be very affordable in terms

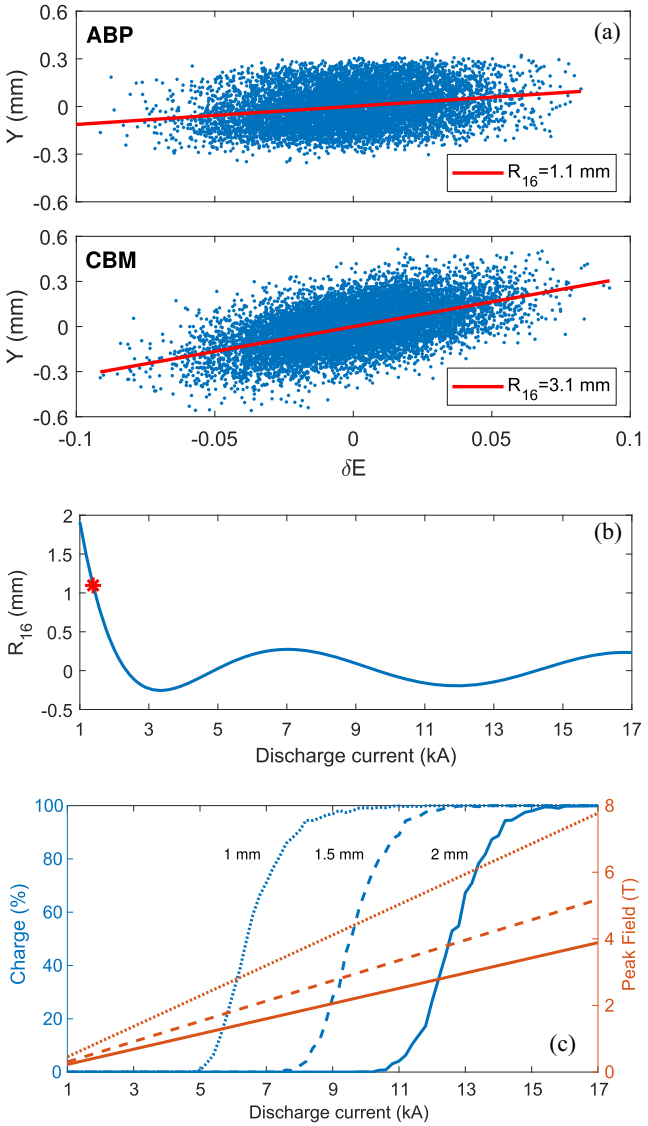

FIG. 5. (a) Chromatic dispersion downstream the ABP and CBM. The x axis represents the particle energy deviation δE with respect to the central beam energy E while the y axis shows the particle position Y. The R_{16} transport matrix element is obtained from the linear fit. (b) Evaluation of the R_{16} as a function of the discharge current. The red asterisk shows the R_{16} computed with the maximum discharge current used in the experiment. (c) Scalability of the ABP to larger beam energies. Guiding efficiency (percentage of transported charge, blue lines) of a 1 GeV beam for several discharge currents and three capillary diameters. The corresponding peak magnetic fields (red lines) are also reported.

of size and costs. The ABP represents therefore an innovative solution to develop ultracompact beam lines for existing or next-generation accelerator facilities.

The data that support the findings of this study are available from the corresponding author on reasonable request.

This work has has received funding from the European Union's Horizon Europe research and innovation programme under Grant Agreement No. 101079773 (EuPRAXIA Preparatory Phase) and the INFN with the Grant No. GRANT73/PLADIP. We thank G. Grilli and T. De Nardis for the development of the HV discharge pulser, F. Anelli for the technical support and M. Zottola for the experimental chamber installation. We also thank all the machine operators involved in the experimental run.

The authors declare no competing interests.

*Corresponding author: riccardo.pompili@lnf.infn.it

[1] H. Yoneda *et al.*, Nature (London) **524**, 446 (2015).
[2] P. K. Maroju *et al.*, Nature (London) **578**, 386 (2020).
[3] T. Tajima and J. M. Dawson, Phys. Rev. Lett. **43**, 267 (1979).
[4] V. Malka *et al.*, Science **298**, 1596 (2002).
[5] S. P. Mangles *et al.*, Nature (London) **431**, 535 (2004).
[6] J. Faure, Y. Glinec, A. Pukhov, S. Kiselev, S. Gordienko, E. Lefebvre, J.-P. Rousseau, F. Burgy, and V. Malka, Nature (London) **431**, 541 (2004).
[7] I. Blumenfeld *et al.*, Nature (London) **445**, 741 (2007).
[8] AWAKE Collaboration, Nature (London) **561**, 363 (2018).
[9] A. Gonsalves, K. Nakamura, J. Daniels, C. Benedetti, C. Pieronek *et al.*, Phys. Rev. Lett. **122**, 084801 (2019).
[10] A. Deng *et al.*, Nat. Phys. **15**, 1156 (2019).
[11] R. Pompili *et al.*, Nat. Phys. **17**, 499 (2021).
[12] C. A. Lindstrøm, J. M. Garland, S. Schröder, L. Boulton, G. Boyle *et al.*, Phys. Rev. Lett. **126**, 014801 (2021).
[13] W. Wang *et al.*, Nature (London) **595**, 516 (2021).
[14] R. Pompili *et al.*, Nature (London) **605**, 659 (2022).
[15] M. Galletti, D. Alesini, M. P. Anania, S. Arjmand, M. Behtouei *et al.*, Phys. Rev. Lett. **129**, 234801 (2022).
[16] M. Labat *et al.*, Nat. Photonics **17**, 150 (2023).
[17] G. White *et al.*, J. Instrum. **17**, P05042 (2022).
[18] J. Lim, P. Frigola, G. Travish, J. B. Rosenzweig, S. G. Anderson, W. J. Brown, J. S. Jacob, C. L. Robbins, and A. M. Tremaine, Phys. Rev. ST Accel. Beams **8**, 072401 (2005).
[19] T. Watanabe, T. Taniuchi, S. Takano, T. Aoki, and K. Fukami, Phys. Rev. Accel. Beams **20**, 072401 (2017).
[20] E. Todesco, B. Bellesia, L. Bottura, A. Devred, V. Remondino, S. Pauletta, S. Sanfilippo, W. Scandale, C. Vollinger, and E. Wildner, IEEE Trans. Appl. Supercond. **14**, 177 (2004).
[21] L. Rossi and L. Bottura, Rev. Accel. Sci. Techol. **05**, 51 (2012).
[22] L. Evans and P. Bryant, J. Instrum. **3**, S08001 (2008).
[23] R. Pompili, G. Castorina, M. Ferrario, A. Marocchino, and A. Zigler, AIP Adv. **8**, 015326 (2018).
[24] R. Pompili, M. P. Anania, M. Bellaveglia, A. Biagioni, S. Bini *et al.*, Phys. Rev. Lett. **121**, 174801 (2018).
[25] M. Ferrario *et al.*, Nucl. Instrum. Methods Phys. Res., Sect. B **309**, 183 (2013).
[26] R. Pompili *et al.*, New J. Phys. **18**, 083033 (2016).
[27] A. Biagioni *et al.*, Plasma Phys. Control. Fusion **63**, 115013 (2021).
[28] M. Galletti *et al.*, Symmetry **14**, 450 (2022).
[29] A. Biagioni *et al.*, J. Instrum. **14**, C03002 (2019).
[30] N. A. Bobrova, A. A. Esaulov, J.-I. Sakai, P. V. Sasorov, D. J. Spence, A. Butler, S. M. Hooker, and S. V. Bulanov, Phys. Rev. E **65**, 016407 (2001).
[31] R. Pompili *et al.*, Appl. Phys. Lett. **110**, 104101 (2017).
[32] M. Reiser, *Theory and Design of Charged Particle Beams* (John Wiley & Sons, New York, 2008).
[33] J. J. Rocca, O. D. Cortázar, B. Szapiro, K. Floyd, and F. G. Tomasel, Phys. Rev. E **47**, 1299 (1993).
[34] A. Ben-Kish, M. Shuker, R. A. Nemirovsky, A. Fisher, A. Ron, and J. L. Schwob, Phys. Rev. Lett. **87**, 015002 (2001).
[35] R. England, J. B. Rosenzweig, G. Andonian, P. Musumeci, G. Travish, and R. Yoder, Phys. Rev. ST Accel. Beams **8**, 012801 (2005).
[36] R. Assmann *et al.*, Eur. Phys. J. Spec. Top. **229**, 3675 (2020).
[37] M. Ferrario *et al.*, Nucl. Instrum. Methods Phys. Res., Sect. A **909**, 134 (2018).